doi:10.1016/j.jmb.2010.09.020 J. Mol. Biol. (2010) 403, 546–561

Contents lists available at www.sciencedirect.com

Journal of Molecular Biology

journal homepage: http://ees.elsevier.com.jmb

Cellular Architecture of *Treponema pallidum*: Novel Flagellum, Periplasmic Cone, and Cell Envelope as Revealed by Cryo Electron Tomography

Jun Liu[1]*, Jerrilyn K. Howell[1], Sherille D. Bradley[1], Yesha Zheng[1], Z. Hong Zhou[2] and Steven J. Norris[1,3]

[1]*Department of Pathology and Laboratory Medicine, University of Texas Medical School at Houston, 6431 Fannin, MSB 2.228, Houston, TX 77030, USA*
[2]*Department of Microbiology, Immunology, and Molecular Genetics, University of California, Los Angeles, Los Angeles, CA, USA*
[3]*Department of Microbiology and Molecular Genetics, University of Texas Medical School at Houston, Houston, TX 77030, USA*

Received 4 July 2010; received in revised form 2 September 2010; accepted 9 September 2010
Available online 17 September 2010

Edited by W. Baumeister

Keywords:
cryo electron tomography; cell envelope architecture; syphilis spirochete; periplasmic flagellum; bacterial structure

High-resolution cryo electron tomography (cryo-ET) was utilized to visualize *Treponema pallidum*, the causative agent of syphilis, at the molecular level. Three-dimensional (3D) reconstructions from 304 infectious organisms revealed unprecedented cellular structures of this unusual member of the spirochetal family. High-resolution cryo-ET reconstructions provided detailed structures of the cell envelope, which is significantly different from that of Gram-negative bacteria. The 4-nm lipid bilayer of both outer membrane and cytoplasmic membrane resolved in 3D reconstructions, providing an important marker for interpreting membrane-associated structures. Abundant lipoproteins cover the outer leaflet of the cytoplasmic membrane, in contrast to the rare outer membrane proteins visible by scanning probe microscopy. High-resolution cryo-ET images also provided the first observation of *T. pallidum* chemoreceptor arrays, as well as structural details of the periplasmically located cone-shaped structure at both ends of the bacterium. Furthermore, 3D subvolume averages of periplasmic flagellar motors and flagellar filaments from living organisms revealed the novel flagellar architectures that may facilitate their rotation within the confining periplasmic space. Our findings provide the most detailed structural understanding of periplasmic flagella and the surrounding cell envelope, which enable this enigmatic bacterium to efficiently penetrate tissue and to escape host immune responses.

Introduction

Treponema pallidum subsp. *pallidum* is the causative agent of syphilis, a sexually transmitted disease with more than 12 million new cases worldwide each year.[1] Since 2000, the reported cases of primary syphilis and secondary syphilis have been rising annually in the United States.[2] Of major concern is the recognition that syphilis infection greatly increases

*Corresponding author. E-mail address: Jun.Liu.1@uth.tmc.edu.

Abbreviations used: cryo-ET, cryo electron tomography; 3D, three-dimensional; SPM, scanning probe microscopy; PBS, phosphate-buffered saline; BSA, bovine serum albumin.

susceptibility to human immunodeficiency virus infection.[3] In addition, closely related organisms cause endemic syphilis (*T. pallidum* subsp. *endemicum*), yaws (*T. pallidum* subsp. *pertenue*), pinta (*Treponema carateum*), and venereal spirochetosis in rabbits (*Treponema paraluiscuniculi*).[4] The genome sequences of several of these organisms have been determined.[5,6] *T. pallidum* continues to be an enigmatic pathogen because of the lack of readily identifiable virulence determinants and the poorly understood pathogenesis of the disease. This deficiency is due primarily to the inability to culture members of this group of obligate pathogens continuously *in vitro*.[7]

T. pallidum is a member of the Spirochaetaceae, a biomedically important bacterial phylum that includes the etiological agents of Lyme disease (*Borrelia burgdorferi*)[8] and leptospirosis (*Leptospira interrogans*).[9] A striking feature of *T. pallidum* and other spirochetes is their capacity to swim efficiently in a highly viscous gel-like environment, such as connective tissues, where most externally flagellated bacteria are slowed or stopped.[10] Therefore, motility is likely to play an important role in the widespread dissemination of spirochetal infections and in the establishment of chronic disease.[10,11] Motility-associated genes are shared by both *T. pallidum* and *B. burgdorferi*, and an in-depth comparative analysis of these spirochetes may greatly enhance our understanding of the fundamental physiology of these important pathogens.[5,12]

T. pallidum has a spiral shape with a length ranging from 6 μm to 15 μm and a diameter of ~0.2 μm.[11,13–16] The protoplasmic cylinder is surrounded by a cytoplasmic membrane, which is enclosed by a loosely associated outer membrane. A thin layer of peptidoglycan between the membranes provides structural stability while permitting flexibility. The flagella are located in the periplasmic space, between the cytoplasmic membrane and the outer membrane. Bundles of flagella originate from flagellar motors at both ends of the organism, wind around the flexible protoplasmic cell cylinder, and overlap in the middle. *T. pallidum* contains multiple chemotaxis genes encoding methyl-accepting chemotaxis proteins.[5] *Treponema* species also contains cytoplasmic filaments arranged in a ribbon configuration that spans the entire length of the cell.[17–20] *cfpA*, the gene encoding the ~79-kDa major subunit of the cytoplasmic filaments, is highly conserved in *Treponema* species. In *Treponema denticola* or *Treponema phagedenis*, mutation of *cfpA* results in defective cell division in which two or more cytoplasmic cylinders are encased in a single outer membrane.[17] There are at least 46 putative lipoproteins in *T. pallidum*;[21] other than the 47-kDa carboxypeptidase and multiple ABC transporter periplasmic binding proteins, the functions of these lipoproteins are largely unknown.[11] *T. pallidum* also has a paucity of integral membrane proteins in its outer membrane and has been referred to as the "stealth pathogen" because of the scarcity of antigens on its outer surface.[2,22,23]

Flagella play an essential role in the motility, morphology, and biology of spirochetes and other organisms.[10] Flagellar structure and function have been extensively studied using *Escherichia coli* and *Salmonella enterica* as model systems. Flagellar motion is powered by a proton-driven or sodium-ion-driven rotary motor embedded in the cytoplasmic membrane, but the precise mechanisms of flagellar motor rotation and reversal remain to be determined.[24–28] The periplasmic flagellar assemblies of *T. pallidum* are expected to generally resemble those of external flagella, owing to the high degree of similarity between flagellar gene homologs. In recent years, there has been progress in understanding the periplasmic-flagella-driven motility of *B. burgdorferi* and other spirochetes.[29] The motility of *B. burgdorferi* results from the coordinated asymmetric rotation of the flagella at both ends of the cell.[30] The *T. pallidum* flagellar filaments are composed of several major proteins, including flagellar core proteins FlaB1, FlaB2, and FlaB3, and the sheath protein FlaA.[31–33] However, the structural details of periplasmic flagella remain unknown.

The cellular architectures of several spirochetes (including *T. pallidum*, *Treponema primitia*, *T. denticola*, and *B. burgdorferi*) have been studied extensively using cryo electron tomography (cryo-ET) analysis.[34–37] Cryo-ET has emerged as a three-dimensional (3D) imaging technique used to visualize cellular and subcellular structures at the molecular level.[38,39] The distinct advantage of cryo-ET is its potential to elucidate the structure of cellular components *in situ* without fixation, dehydration, embedding, or sectioning artifacts. The power of cryo-ET has been significantly enhanced by 3D subvolume averaging and classification techniques.[40–43] We recently used high-throughput cryo-ET of *B. burgdorferi* to determine the molecular architecture of intact flagellar motor at a resolution of 3.5 nm.[44]

In this study, we investigated infectious *T. pallidum* organisms and their periplasmic flagella *in situ* by utilizing high-throughput cryo-ET. Cryo-ET reconstructions from 304 frozen–hydrated organisms generally support the recently published results of Izard *et al.* but provide a significant amount of novel structural information regarding the detailed structures of the cell envelope, the localization of chemoreceptor arrays, and the molecular architecture of flagellar filaments and flagellar motors *in situ*.[35] Abundant lipoproteins studding the outer leaflet of the cytoplasmic membrane were visualized for the first time; the proteinaceous nature of this layer was verified by its dissolution following proteinase K treatment of partially disrupted organisms. A periplasmically located cone-shaped structure was observed at the ends of each organism; this unique

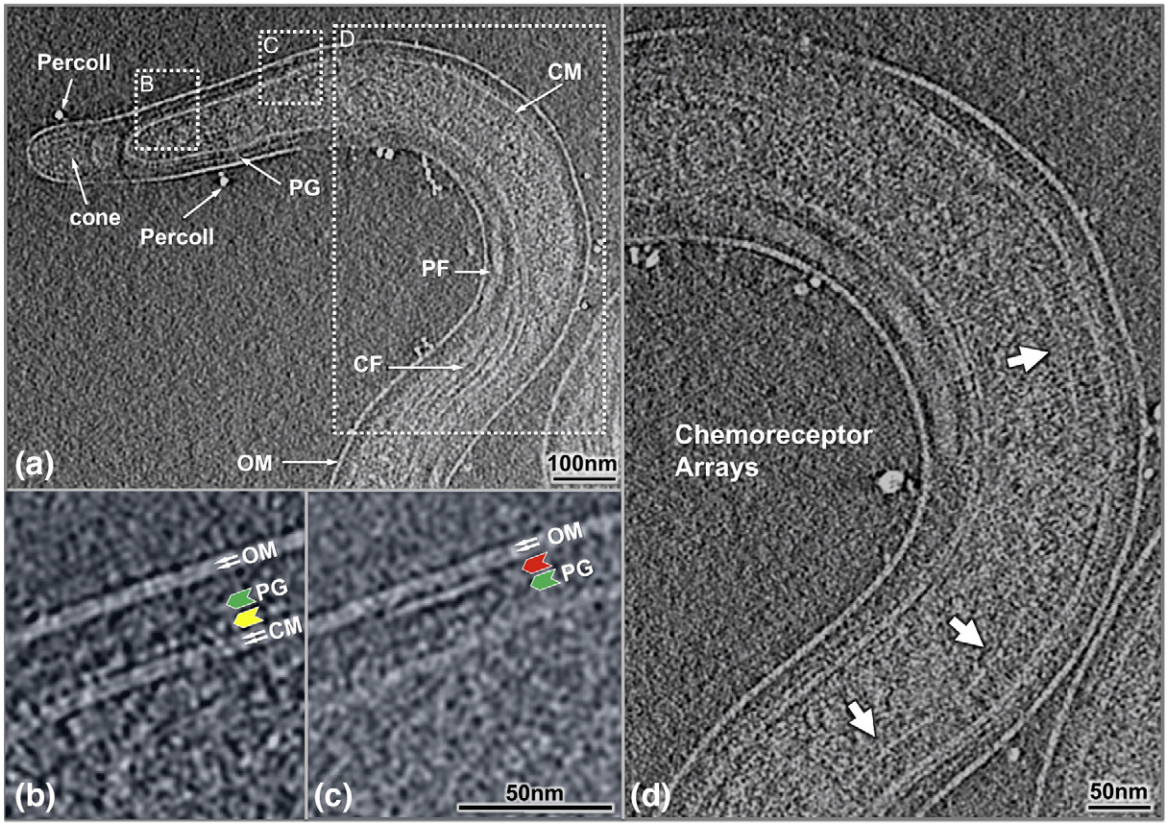

Fig. 1. Cellular architecture of an intact *T. pallidum* cell. (a) A typical tomographic slice near the center of the bacterium after a 4×4 binning of the original reconstruction. The prominent structural features include the outer membrane, cytoplasmic membrane, peptidoglycan layer, periplasmic flagella, and cytoplasmic filaments (a). The outlined region on the left (a) is enlarged in (b) after a 2×2 binning of the original reconstruction. The dotted outline on the right (a) is enlarged in (c). The two leaflets of the membranes are visible, as indicated by white arrows. The extra layer of density adjacent to the cytoplasmic membrane is indicated by a yellow arrow, whereas the apparent peptidoglycan layer is shown by a green arrow. An example of a patch of density associated with the inner leaflet of the outer membrane is marked by a red arrow (c). Examples of structures resembling chemoreceptor arrays are visible in (d) (white arrows).

feature appears to be composed of lipoproteins arranged in a helical lattice adjacent to the outer membrane. Furthermore, a comparative analysis of *B. burgdorferi* and *T. pallidum* provides insight into the common cellular structures of spirochetes and also exhibits some unique pathogenesis-related features of these two pathogens.

Results

Cryo-ET of intact *T. pallidum* cells

T. pallidum cells ($n=304$) were imaged under optimal conditions to obtain high-resolution structures using high-throughput cryo-ET. The organism typically tapers from an approximate diameter of 0.2 μm to 0.1 μm near the end of the cell, as shown in a representative image (Fig. 1a). Similar to *B. burgdorferi* and other spirochetes examined previously, the image from a *T. pallidum* cell (Fig. 1a) illustrates the outer membrane, the cytoplasmic membrane, and a thin peptidoglycan layer, with the flagella wrapping around the cell body in the periplasmic space. Enlarged views (Fig. 1b and c) reveal the inner and outer leaflets of the lipid bilayer of both the outer membrane and the cytoplasmic membrane. The *T. pallidum* outer membrane appears as a simple lipid bilayer by cryo-ET. It therefore differs substantially from the outer membrane of *B. burgdorferi*, which has a contiguous external layer of density attributable to surface lipoproteins.[44] In contrast, a contiguous layer of density associated with the outer surface of the cytoplasmic membrane was demonstrable in most cryo-ET sections of *T. pallidum* (Fig. 1b, yellow arrow). This layer was distinct from the more loosely arranged density located near the middle of the periplasm (Fig. 1b, green arrow), which represents the peptidoglycan layer. The punctuate nature of the cytoplasmic-membrane-proximal density, along with

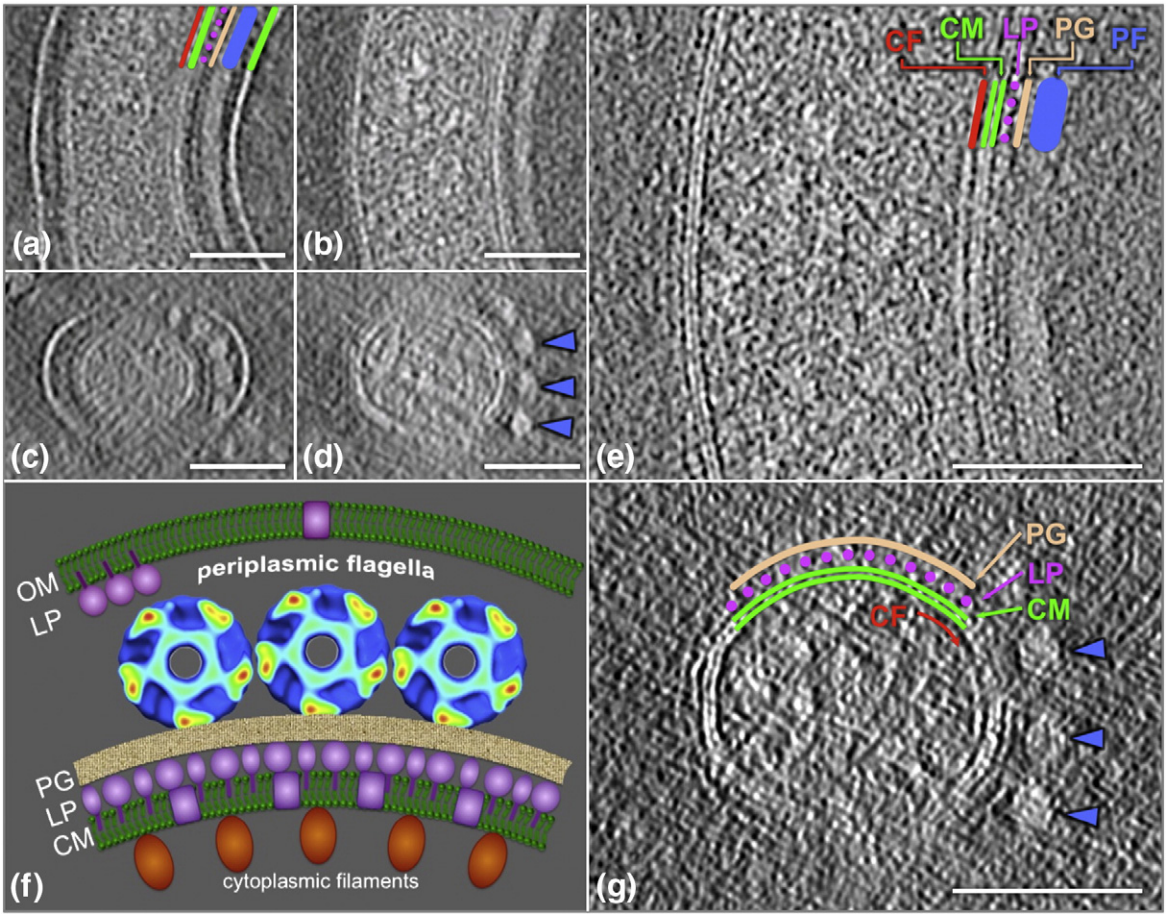

Fig. 2. The *T. pallidum* cell envelope architecture. The space between the outer membrane and the cytoplasmic membrane increases from ~23 nm to ~49 nm in regions containing the periplasmic flagella (a and c). The periplasmic flagella (blue line) remain closely associated with the cell cylinder following removal of the outer membrane through repeated centrifugation (b and d). The 4-nm lipid bilayer composition of the cytoplasmic membrane is visible in higher-magnification views (e and g). The locations of the cytoplasmic filaments (red line), lipoprotein layer (purple circles), and peptidoglycan (tan line) are indicated (e). (a), (b), and (e) are longitudinal views, while (c) and (d) are cross-sectional views. The putative layer of lipoproteins (purple) appeared to be on the cytoplasmic membrane (CM) and to be just underneath the thin layer of peptidoglycan (PG). A model of *T. pallidum* cell envelope is shown in (f). Rare outer membrane proteins (purple) are exposed on the outer membrane (OM).

frequent interconnections with the outer leaflet, suggests that this layer may represent periplasmic lipoproteins anchored to the cytoplasmic membrane (Fig. 1b, yellow arrow). In addition, there are small patches of proteins extending from the inner leaflet of the outer membrane (Fig. 1c, red arrow). The occasional dense particles observed outside the organism are residual Percoll particles from the *T. pallidum* purification procedure.

Putative chemoreceptor arrays were directly visualized for the first time in *T. pallidum* organisms, as exemplified in Fig. 1d. There are three arrays visible in this reconstruction. Their locations are variable, typically from 500 nm to 1000 nm away from the cell end. The width of the arrays is also variable; however, the height of the receptor (from a prominent line "base plate" to the cell membrane) is relatively consistent at ~27 nm. Although the detailed structure of the *T. pallidum* chemoreceptor array has not been determined yet, it appears to be similar to the characteristic structure of bacterial chemoreceptors observed to date.[45]

Characterization of cell envelope

The appearance of the cell envelope of *T. pallidum* is modulated by the intertwining of the periplasmic flagellar ribbon. The space between the cytoplasmic membrane and the outer membrane was typically ~23 nm and became wider (up to 49 nm) in the vicinity of periplasmic flagella (20 nm in diameter), as shown in Fig. 2a and c. By repeated centrifugation and

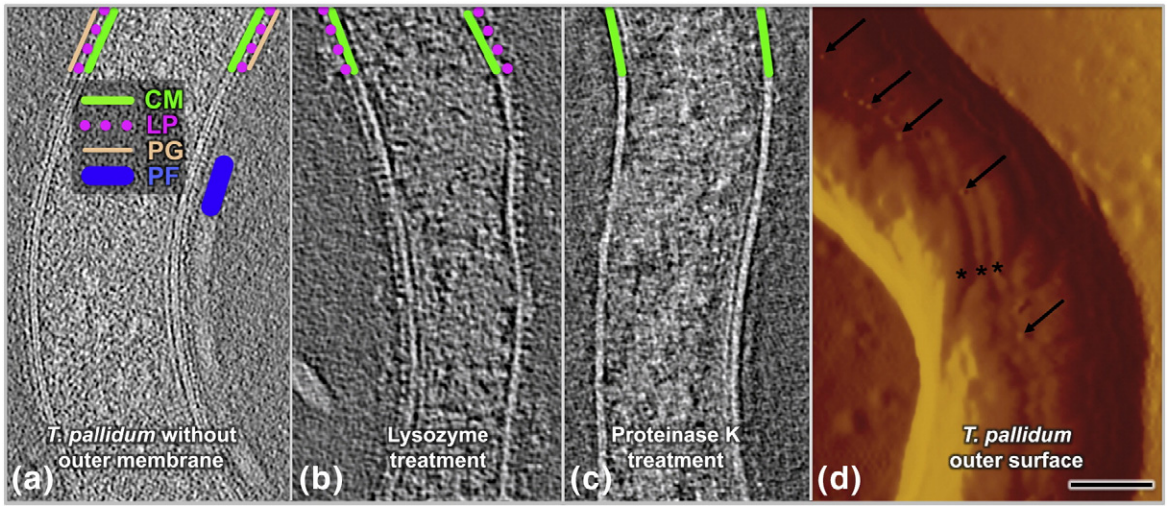

Fig. 3. Confirmation of *T. pallidum* peptidoglycan layer, cytoplasmic membrane surface proteins, and rare outer surface proteins. Cells in all panels were previously treated with distilled water to remove the outer membrane and to expose subsurface structures. (a) Cells without subsequent enzyme treatment. The locations of the cytoplasmic membrane (green line), surface proteins (purple circles), peptidoglycan (orange line), and a periplasmic flagellum (blue line) are shown. (b) With lysozyme treatment. The peptidoglycan layer was removed, whereas the putative lipoproteins (purple circles) are still visible on the outer surface of the cytoplasmic membrane (c) With proteinase K treatment, the layer of putative lipoproteins was removed. (d) The presence of intramembranous particles on the outer surface of *T. pallidum*, as revealed by SPM. Freshly prepared Percoll-purified *T. pallidum* was applied to a mica surface, air dried, and visualized by SPM. A portion of one *T. pallidum* cell is shown in amplitude mode. Small protrusions are visible on the outer surface (arrows) and often are located on the bulge in the outer membrane created by the underlying periplasmic flagella (asterisks). The scale bar represents 100 nm.

resuspension of *T. pallidum*, the outer membrane can be removed gently without disrupting the association between the flagella and the cell cylinder (Fig. 2b and d). Higher-magnification views of this organism reveal the structural details around the cytoplasmic membrane bilayer, which is visible as parallel densities spaced 4 nm apart (Fig. 2e and g). An array of cytoplasmic filaments lies just underneath the inner surface of the cytoplasmic membrane, as subsequently described in greater detail. There are two layers of densities in close proximity to the periplasmic side of the cytoplasmic membrane (Fig. 2e and g). The inner layer (Fig. 2e and g, purple) appears to consist of a discontinuous array of discrete particles that extend from the outer leaflet of the cytoplasmic membrane. This series of 'studs' was suggestive of a layer of proteins that are anchored to the cytoplasmic membrane through either lipid moieties or hydrophobic amino acid domains. The more distal layer (Fig. 2e and g, tan), which lies between the 'stud' layer and the periplasmic flagella, is more contiguous and appears to correspond to the peptidoglycan layer.

To delineate the composition of these cytoplasmic-membrane-proximal layers, we partially disrupted *T. pallidum* cells by repeated centrifugation and resuspension to remove the outer membrane and thus provide access to periplasmic components for treatment with lysozyme or proteinase K (Fig. 3). In prior studies, it had been shown that repeated centrifugation and resuspension of Percoll-purified *T. pallidum* in distilled water resulted in blebbing and release of the outer membrane from the majority of cells.[20] We thus treated cells in a similar manner prior to addition of lysozyme or proteinase K. The suspected membrane protein and peptidoglycan layers, as well as the periplasmic flagella and cytoplasmic filaments, were still clearly preserved in repeatedly centrifuged specimens (Fig. 3a). Following treatment with lysozyme, the proposed peptidoglycan layer was removed, whereas the layer of protrusions proximal to the cytoplasmic membrane remained intact (Fig. 3b). In contrast, treatment with proteinase K resulted in complete removal of this cytoplasmic-membrane-proximal 'stud' layer (Fig. 3c). This analysis confirmed the presence of a prominent layer of proteins next to the cytoplasmic membrane, followed by a thin peptidoglycan layer. We propose that the protein layer is composed primarily of lipoproteins, given the abundance of lipoproteins in *T. pallidum*.[5]

Our cryo-ET studies corroborated numerous prior studies indicating that the *T. pallidum* outer membrane lacks proteins or other structures that extend from the membrane bilayer. The treponemal rare outer membrane proteins (also called TROMPs) that appear to represent integral membrane proteins were

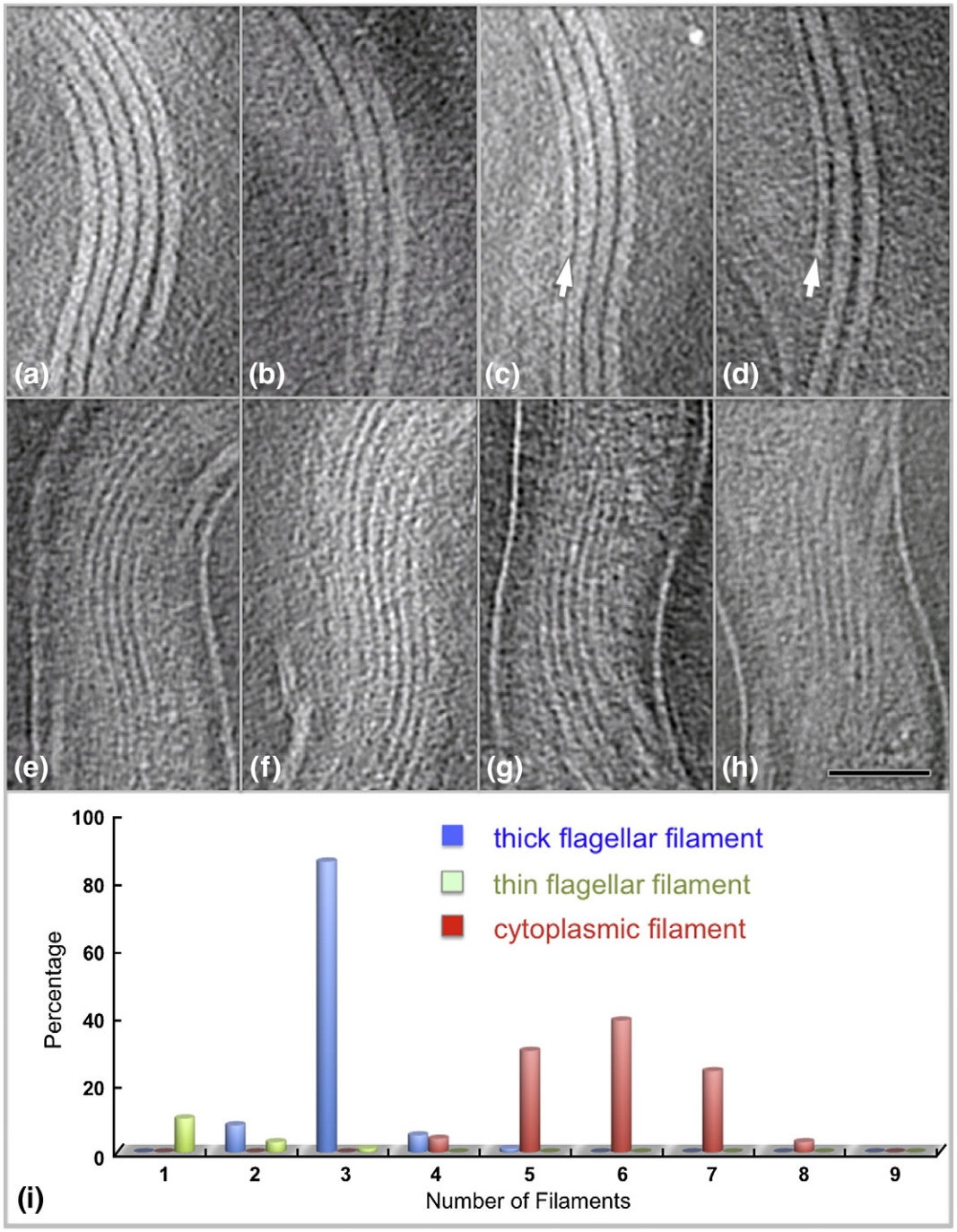

Fig. 4. Morphology and distribution of periplasmic flagella and cytoplasmic filaments. The flagella form a side-by-side ribbon that wraps around the protoplasmic cylinder in a right-handed fashion (a–d). The diameter of flagella is ~20 nm. In addition, a thin periplasmic filament is occasionally associated with the flagellar ribbon (c and d), as indicated by a white arrow. The diameter of the thin filament is ~13 nm. Cytoplasmic filaments (e–h) form a ribbon-type structure located within the protoplasmic cylinder. The cytoplasmic filaments are parallel with the periplasmic flagella. The scale bar represents 100 nm. The number of filaments per cell is depicted in (i) and is based on the cryo-ET analysis of 304 cells. The number of flagellar filaments is narrowly distributed, with a large majority (86%) of cells possessing three flagella per cell end (blue). The number of cytoplasmic filaments is distributed in a slightly larger range from four to eight (red). The thin periplasmic filaments exist at a low frequency (about one of eight cells), and one to three thin filaments are visible in these organisms (light green).

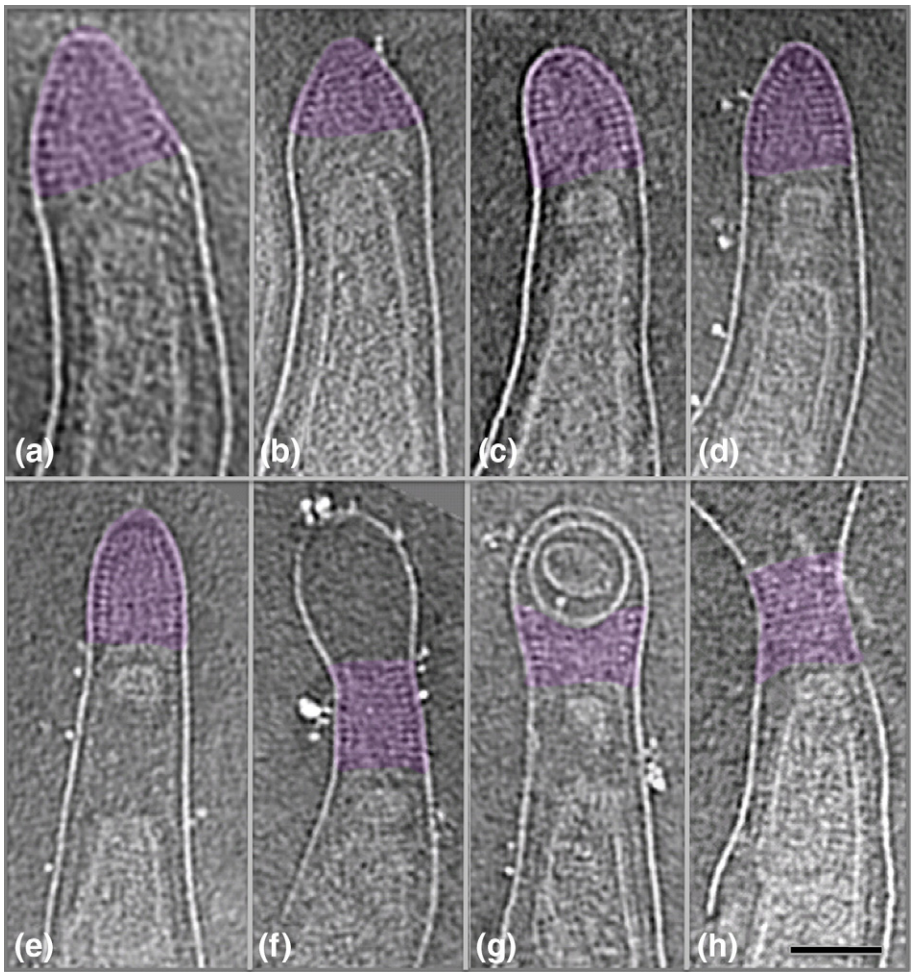

Fig. 5. Cone-shaped structures located at the ends of *T. pallidum*. A helical or ring-shaped array forms the outer surface of a cone-shaped structure (purple) at both ends of the organism (a–h). It appears that the structure is likely associated with the outer membrane. Membrane-delimited vesicles are sometimes localized distal or (more commonly) proximal to the cone. The scale bar represents 100 nm.

not readily visible by cryo-ET. For further examination of the *T. pallidum* surface structure, freshly prepared *T. pallidum* was applied to a mica surface, air dried, and analyzed using scanning probe microscopy (SPM), a technique that provides high-resolution 3D images of surface topology.[46] SPM revealed the presence of occasional protrusions (marked by arrows) on the *T. pallidum* cell surface (Fig. 3d). Some of these protrusions were located in the outer membrane overlying the periplasmic flagella (asterisks). These protrusions (~8 nm in diameter) appear to correspond to *T. pallidum* rare outer membrane proteins, identified previously by freeze-fracture microscopy as ~ 11-nm intramembranous particles.[15,16,47] As noted previously, these densities tend to overlie the periplasmic flagella, which are visible as three ridges (marked with asterisks) in Fig. 3d. The protrusions are structurally distinct from the much larger and randomly distributed Percoll particles shown in Fig. 1.

Periplasmic flagella

The flagellar filaments extend from each flagellar motor and are clearly localized between the peptidoglycan layer and the outer membrane (Fig. 2a and b). The diameter of the filament is approximately 20 nm. Flagellar filaments typically form a parallel array (Fig. 4a–d), with each filament becoming associated with others beyond the hook region. The center-to-center distance between two filaments is slightly larger than 20 nm. Most bacteria (86%) exhibited three flagella at each end of the organism, although a few had two, four or five flagella (Fig. 4a, b, and i). Thin filaments were also visible in approximately one of eight cells (Fig. 4c, d, and i). The diameter of these thin filaments was ~13 nm, in contrast to the 20-nm-'thick' flagellar filament. Each of the 'standard' 20-nm flagellar filaments was connected to an intact flagellar motor (Fig. S1), whereas the 'thin' filaments examined were not

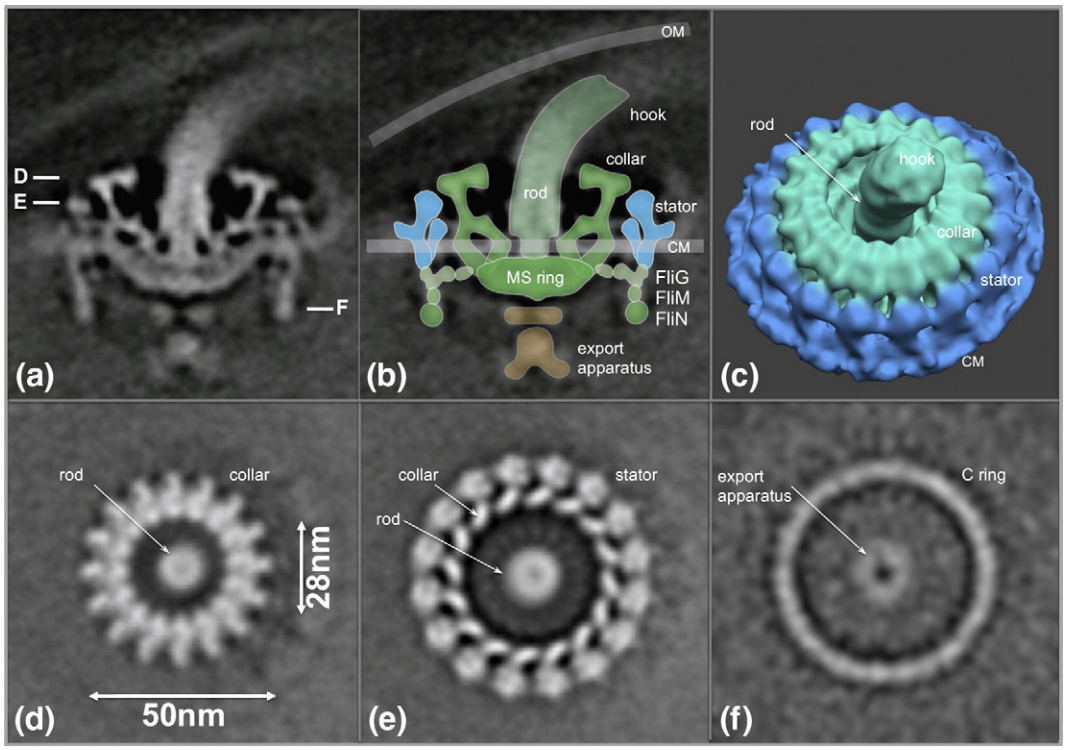

Fig. 6. Molecular architecture of the intact flagellar motor. (a) Central section of an asymmetric 3D average structure of the flagellar motor. (b) A provisional flagellar motor model is overlaid on the image in (a); proposed locations of the underlying structures are indicated in c–f. (c) Surface rendering of the flagellar motor structure (the rotor is shown in green, and the stator is shown in cyan). (d–f) Horizontal cross sections through a flagellar motor. Section D is located near the top of the motor; the central rod and the uppermost portion of the rotor are visible. Section E transects the middle of the rotor body and the stator, just above the cytoplasmic membrane. The bottom of the C ring is visible in section F. A portion of the export apparatus is visible in the center of the C ring. The scale bar represents 50 nm.

obviously associated with flagellar motors or any other discernible molecular assembly. Immunogold labeling of periplasmic flagella from partially disrupted organisms of *T. pallidum* demonstrated that FlaA antibodies bind to the surface of thick filaments, while FlaB1 antibodies bind preferentially to the thin filaments (Fig. S2). Therefore, the thick filaments (20 nm in diameter) are likely composed of FlaB subunits in the core and FlaA on the surface, whereas thin filaments (13 nm in diameter) are apparently composed of FlaB subunits.

Cytoplasmic filaments

The cytoplasmic filaments form a ribbon (Fig. 4e–h) underneath the cytoplasmic membrane with a width of 7.0–7.5 nm. The distance between the filaments is about 13.0 nm. The number of cytoplasmic filaments ranges from four to eight per cell, but most cell sections containing six filaments on average (Fig. 4i). The 3D reconstructions of the different regions of the cell body indicated that the cytoplasmic filament ribbon runs parallel with the periplasmic flagellar ribbon, separated by the cytoplasmic membrane and the peptidoglycan layer (Fig. 2f).

Cone-shaped structure

A periplasmically located cone-shaped structure was found at the end of every organism (Fig. 5, purple). The cone-shaped structure is located adjacent to the outer membrane and sometimes 100 nm away from the cytoplasmic membrane (Fig. 5d and e). It appears that one or more proteins (most likely including at least one lipoprotein) form a helical or ring-shaped lattice along the inner surface of the outer membrane, with a longitudinal spacing of ~5 nm between neighboring lattices. The inner portion of the cone structure was relatively amorphous, with no clear arrangement of densities.

Molecular architecture of the intact flagellar motor

Three flagellar motors are typically located at each end of the bacterium (Fig. 4i). In individual tomograms, an architecture resembling a bowl-shaped structure surrounding a central rod could be discerned (Fig. S1b and d). A 3D reconstruction of the intact flagellar motor without imposed symmetry was obtained from the subvolume alignment and

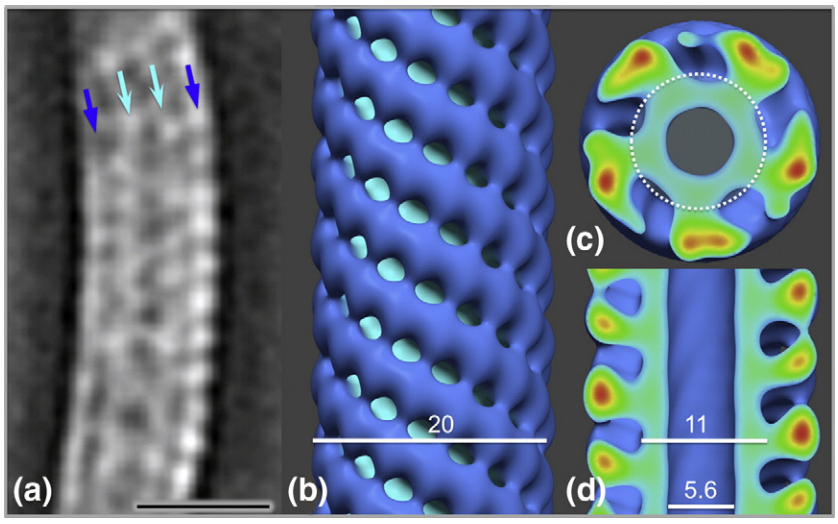

Fig. 7. Structural characterization of periplasmic flagella *in situ*. A single slice from the averaged map of periplasmic flagellar (thick filament) segments illustrates the curved configuration of their superhelical conformation (a). After mathematical 'straightening' of the superhelical curvature, the refined structural model of the periplasmic flagella in surface view (b) and of center sections (c and d) reveals the central channel, the filament core, and its surrounding protein sheath. The scale bar represents 20 nm.

averaging of 830 motors. A central section of the resulting 3D construct illustrates the locations of the putative hook, rod, MS ring, stator, C ring, and export apparatus structures (Fig. 6a).

The hook structure is visible at the top, attached to the central rod. The rod has a central channel, as noted in the flagellar motor from *B. burgdorferi*.[44] The 16-fold symmetry of the outer portion of the upper region of the motor is clearly evident in the cross sections shown in Fig. 6d and e. The centrally located export apparatus is visible on the cytoplasmic side of the MS ring (Fig. 6a and f). The most peripherally located elements of the motor (shown in cyan in the surface view of the *T. pallidum* flagellar motor, as shown in Fig. 6c) are thought to represent the stator, which is composed of the membrane-associated proteins MotA and MotB and is embedded in the cytoplasmic membrane (Fig. 6b and c). Overall, the structure of the *T. pallidum* flagellar motor closely resembles those of *B. burgdorferi*[44] and *T. primitia*.[48]

Differences between the *T. pallidum* structure and the *B. burgdorferi* structure do exist. In the *T. pallidum* motor, the top of the collar extends further inward toward the rod, such that the 'opening' of the collar is ~28 nm; by comparison, the opening for the *B. burgdorferi* collar is ~38 nm.[44] In addition, the *T. pallidum* rotor lacks the torus-shaped ring corresponding to FlgI in *B. burgdorferi*; this result is consistent with the absence of *flgI* in the *T. pallidum* genome.[5] A model of the relative locations of the stator and the rotor of the *T. pallidum* flagellar motor (Fig. 6b) is proposed based on comparisons with that of *B. burgdorferi*.[44]

Structural characterization of periplasmic flagella

We also carried out a structural characterization of the thick flagellar filament *in situ*. The density maps corresponding to segments of the flagella were aligned to generate the first averaged flagellar filament structure, which revealed its native helical curvature and the characteristic presence of the central and outer layers of density (Fig. 7a). The curved filament structure was 'straightened' to permit longitudinal helical averaging (Fig. 7b–d). The resulting structure revealed a central channel, an inner cylinder of density, and external chains of density in a left-handed five-start helical lattice with a pitch of 6 nm. The central channel and the inner cylinder have diameters of 5.6 nm and 11 nm, respectively (Fig. 7d), whereas the overall diameter of the flagellum is 20 nm. The outer sheath is connected to the core by a narrow region of density and is composed of subunits with a periodicity of 5 nm. The inner core appeared to be composed of five regions of density in each cross section (Fig. 7c); these substructures were tightly arranged in a stacked helical array. Based on our antibody labeling experiments (Fig. S2) and prior studies,[31,49] the inner 'core' (inside the circle outlined in Fig. 7) is likely composed of FlaB subunits, and the outer 'sheath' is composed of FlaA.

Discussion

The pathogenesis of *T. pallidum* is poorly understood at the molecular level, partly due to the inability

to culture the organism continuously *in vitro*. Innovative approaches are consequently needed to study the fundamental biology of this enigmatic spirochete. Cryo-ET is well suited for the elucidation of the 3D cellular architecture of intact organisms at the molecular level. We are able to achieve high-resolution 3D reconstructions of intact organisms under optimal imaging conditions, such as the use of relatively low defocus levels and a small objective aperture. Volume binning of the 3D reconstructions provided additional contrast for visualization of minute structures, including leaflets in membrane bilayers and layers of membrane-associated proteins.

Unique envelope architecture

The cell envelope of *T. pallidum* has been studied extensively using a variety of techniques but remains poorly understood. The high-resolution cryotomographic reconstructions in this study revealed an unprecedented structural detail of the cell envelope. The 4-nm lipid bilayer of both outer membrane and cytoplasmic membrane was resolved by cryo-ET and provided an important marker for the understanding of membrane-associated structures. The outer membrane of *T. pallidum* appears as a simple lipid bilayer, whereas the external surface of the *B. burgdorferi* outer membrane has a clearly visible proteinaceous layer.[44] The *T. pallidum* outer membrane can be removed by centrifugation, suggesting a loose association of this pliable membrane with the underlying structures.

Prior freeze-fracture electron microscopy studies had shown the presence of rare intramembranous particles in the outer membrane, indicating a paucity of membrane-spanning proteins.[15,16,47] We were able to confirm the previously described presence of these treponemal rare outer membrane proteins using SPM, a technique that is complementary to cryo-ET and provides the surface topology of the outer membrane (Fig. 3d). The putative outer membrane proteins appeared to be preferentially distributed over the flagella. We also identified patches of density near the inner surface of the outer membrane, as shown in Fig. 1c (red arrow). These patches may be composed of lipoproteins that are anchored to the inner leaflet of the outer membrane, as has been described for TP453 by Hazlett *et al.*[50] Our data also indicate that the putative lipoprotein layer is closely associated with the cytoplasmic membrane and that the thin peptidoglycan layer lies between this layer of lipoproteins and the periplasmic flagella (Fig. 2f). The space between the cytoplasmic membrane and the outer membrane was wider in the vicinity of periplasmic flagella, as reported in previous studies of *T. pallidum*, *T. denticola*, *T. primitia*, and *B. burgdorferi*.[34–37,51] Together, these structural details help to clarify the previous cell envelope model proposed by Cox *et al.*[52] and Radolf *et al.*[53] The unique surface architecture of *T. pallidum* is significantly different from that of Gram-negative bacteria, but consistent with its remarkable ability to evade the host immune response.[54]

In a recent reanalysis of spirochetal lipoprotein genes, Setubal *et al.* estimated that the *T. pallidum* genome contains 46 genes encoding putative lipoproteins, as compared to 127 predicted lipoprotein genes in *B. burgdorferi*.[21] *B. burgdorferi* has an abundance of lipoproteins anchored on the outer membrane surface, as verified in our previous tomographic studies.[44] However, there is currently no definitive evidence for the surface localization of any *T. pallidum* lipoproteins.[55–58] Several *T. pallidum* proteins have been postulated to be surface exposed based on ligand and/or antibody binding to intact organisms; these candidates include the laminin-binding protein TP0751, the fibronectin-binding and laminin-binding protein TP0136,[58] Tp92, and TprK, a protein that induces opsonic antibodies, undergoes sequence variation, and may promote immune evasion.[54,59] Continued investigation of the *T. pallidum* outer membrane remains critical for an improved understanding of the organism's host–pathogen interactions and for the potential development of vaccines against syphilis.[60]

Unique structure and function of periplasmic flagella

Spirochetes possess periplasmic flagella that confer the ability to effectively translocate under highly viscous gel-like media conditions that would normally hinder other bacteria with external flagella.[10] Unlike most external flagellar filaments, which are composed of a single flagellin subunit, the flagellar filament of *T. pallidum* consists of multiple proteins (FlaB1, FlaB2, FlaB3, and FlaA). Here we provided the first ultrastructure of periplasmic flagella by 3D averaging of the native flagellar filaments (Fig. 7). The flagellar filament structure of *T. pallidum* appears significantly different from the well-known external flagellar filament structure of *S. enterica*[61] and the more recent reconstruction from *Campylobacter jejuni*.[62] The major components of *T. pallidum* flagellar filaments (FlaB1, FlaB2, and FlaB3) are homologous to the N-terminal and C-terminal regions of the flagellins of *S. enterica* and *E. coli*, but their molecular weights are much smaller due to the lack of an ~200-residue domain in the central region of the enteric flagellin sequences.[11] This domain forms an extension out of the filament core in *S. enterica*;[61] this portion of the structure is thus presumed to be absent in the *T. pallidum* flagellar structure.

Prior studies had shown that FlaA forms an external sheath on the *T. pallidum* flagellar filament, whereas FlaB1, FlaB2, and FlaB3 form the central core.[31,49] Our 3D reconstruction of the *T. pallidum* flagellar filament *in situ* (Fig. 7) revealed a central channel surrounded by a core and an outer array of helically arranged

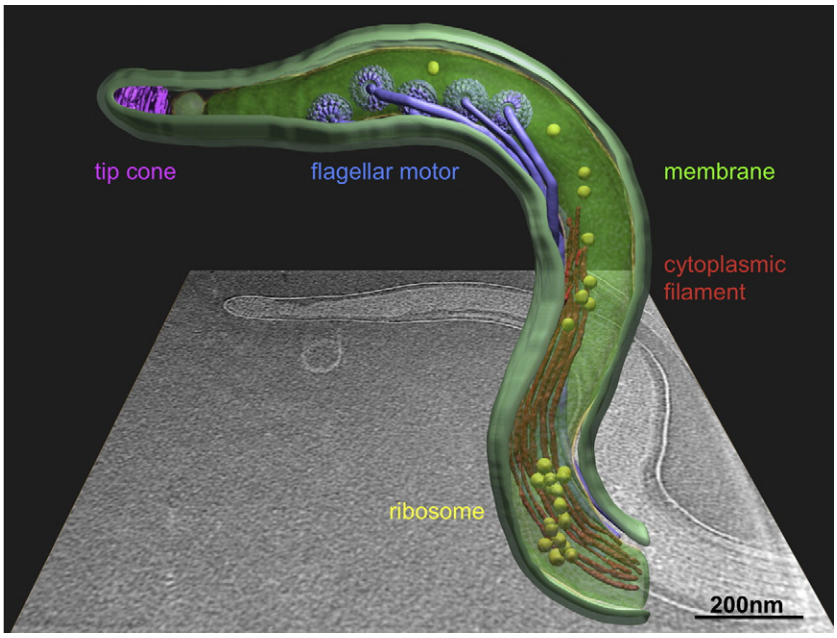

Fig. 8. Cellular architecture of intact *T. pallidum* at the molecular level. One central slice of a tomographic reconstruction from one organism is shown in the background. A 3D model was generated by manually segmenting the outer membrane (light green), cytoplasmic membrane (green), flagellar filaments (blue), cytoplasmic filament (red), cone-shaped structure (magenta), and a large macromolecular complex (yellow). Averaged structures of the flagellar motor were computationally mapped back into their cellular context.

subunits; this structure thus corresponds well with previous findings. The central channel has a diameter of 5.6 nm. A similar channel has been identified in all bacterial flagella examined and is required for the transport of subunits to the flagellar tip during assembly.[61] Our current structural model lacks sufficient detail to determine the arrangement of the FlaB subunits within the core. Cross sections of the model (Fig. 7d) indicate that the filament core (~11 nm in diameter) consists of five regions of density surrounding the central channel; these densities may correspond to individual FlaB polypeptides. Chains of subunits on the outer surface of the flagellum appear to be attached to the core subunits via a narrow stem and thereby follow the helical arrangement of the core. Our data indicate that these chains of subunits represent the outer sheath composed of FlaA. Li *et al.* performed elegant genetic studies in an attempt to delineate the structural roles of the three FlaB proteins and the FlaA subunit of *Serpulina hyodysenteriae*, which has a similar flagellar structure.[63] A *Se. hyodysenteriae flaA* mutant had flagellar filaments with a diameter of 14.8 nm, as compared to a filament diameter of 21 nm in wild-type organisms. This result thus correlates well with our model, with allowance for differences in subunit sizes and measurement methods. In the *Se. hyodysenteriae* studies,[63] the absence of either FlaB1 or FlaB2 resulted in reduced motility and altered the pitch and diameter of the flagellum 'superhelix.' When both genes were mutated, the organisms were nonmotile; purified filaments had lost their superhelical shape and were composed almost entirely of FlaA with little associated FlaB3. Mutations in *flaB3* caused relatively little disruption of flagellar structure and function, indicating that FlaB3 is not essential for flagellar filament assembly.

Three periplasmic flagella typically form a ribbon at each end of *T. pallidum* as they wrap around the cytoplasmic body in right-handed fashion (Fig. 8). Similar results reported in both *B. burgdorferi* and *T. denticola*[34,51] suggest that spirochetes may share similar architectures of flagella or even similar mechanisms of flagellar rotations. In addition to regular flagellar filaments with a diameter of 20 nm, we found that a small proportion of *T. pallidum* cells possessed thin 13-nm filaments. Immunoelectron microscopy (Fig. S2) demonstrated that these thin filaments are composed of FlaB core proteins and appear to lack the sheath component FlaA. While the 20-nm flagella were consistently observed to be connected to motors via a hook structure, the thin filaments did not appear to be associated with flagellar motors. One possibility is that these thin filaments are composed of 'excess' FlaB subunits that are secreted into the periplasmic space and undergo self-assembly.

In examining *B. burgdorferi* by cryo-ET, Charon *et al.* hypothesized that interactions between the flagellar ribbon and the cell cylinder (with peptidoglycan at its outer surface; Fig. 2f) give rise to the formation of the backward-migrating wave in the cell body, thus

imparting the characteristic serpentine movement of spirochetes.[51] Cryo-ET of *T. pallidum* provides a detailed model of the cell envelope with the presence of periplasmic flagella, suggesting that the peptidoglycan layer not only maintains the integrity of the cell cylinder but also serves as the interface between the rotating flagella and the cell cylinder. Without the peptidoglycan layer, the fragile cell body of *T. pallidum* and other spirochetes would not be able to withstand the friction and torque produced by rapid flagellar rotation.

Spirochetal flagellar motor

T. pallidum flagellar motors are anchored on the cytoplasmic membrane at each end of the cell cylinder and are arranged in a row such that the flagellar hooks point toward the middle of the organism (Fig. 8). The flagellar motor operons of *T. pallidum* contain at least 25 genes, most of which are highly homologous to those of *B. burgdorferi* and other spirochetes.[64] The flagellar motors of *T. pallidum* (Fig. 6), *T. primitia*,[48] and *B. burgdorferi*[44] are remarkably similar in their global architecture. One obvious difference is the lack of a P ring in the *T. pallidum* and *T. primitia* motors. This result is consistent with the absence of an *flgI* ortholog in the *T. pallidum* genome.[5] The P ring is clearly not required for motility in *T. pallidum* and *T. primitia*, and previous analyses of *flgI* mutants indicated that the P ring is not required for flagellar rotation in *B. burgdorferi*.[44] In these spirochetes, a collar associated with the rotor forms a characteristic bowl-shaped structure that may replace the putative role of FlgI as a 'bearing' that interacts with the surrounding peptidoglycan layer.[44,48] The collar of the *T. pallidum* motor has a smaller opening compared to the other two spirochetal flagellar motors, which may reflect differences in both protein composition and function. There is currently a lack of information regarding this unique bowl-shaped structure and its function, which may be addressed by additional structural analyses, coupled with gene disruption or labeling studies in genetically tractable organisms such as *B. burgdorferi*, *Se. hyodysenteriae*, and *T. denticola*.[44,63,65]

The morphology of the cytoplasmic filament ribbon

The cytoplasmic filaments of *T. pallidum* form a ribbon-like structure typically composed of four to eight filaments anchored on the inner surface of the cytoplasmic membrane. The ribbon likely extends the length of the cell, as reported in *T. denticola* and *T. phagedenis*.[18] The cytoplasmic filaments of several spirochetes have been purified.[20,66,67] The major component of the cytoplasmic filament is the 79-kDa *cfpA*, which is highly homologous among the treponemes.[66] Based on studies employing *T. denticola* strains in which *cfpA* was disrupted, it has been proposed that the cytoplasmic filament ribbon may be involved in cell division, structural integrity, motility and/or chromosome structure and segregation in *Treponema*.[11,17,19] However, the exact role of cytoplasmic filaments, particularly in *T. pallidum*, requires further investigation.

Cone-shaped structure

The cryo-ET of *T. pallidum*, in this report and in another article recently published by Izard *et al.*,[35] revealed the presence of a previously unrecognized cone-shaped structure located at both ends of the organism (Fig. 5). Several types of 'periplasmic cone' or 'patella-like' structures have been reported previously in *T. primitia* and *T. denticola*.[34,37] Images of the *T. pallidum* cone-shaped structure reported here (Fig. 5) provide additional architectural details and indicate that it is located outside of the peptidoglycan layer and is associated with the outer membrane near the end of the cell. Discrete regularly spaced densities on the outer surface of the cone structure follow the contour of the outer membrane and appear to represent either rings or a helical array of a putative, as yet unidentified protein. The central region of the cone is more amorphous in appearance, indicating that its composition may be different from the outermost aspect of the cone. The association of the cone structure with the outer membrane, as opposed to the cytoplasmic membrane, is demonstrated by its occasional distant localization relative to the end of the cytoplasmic cylinder (e.g., Fig. 5e). What appear to be small cytoplasmic membrane vesicles are often present between the cone-shaped array and the end of the cytoplasmic cylinder. While most commonly located at the cell end, the cone structure is sometimes separated from the end by an outer membrane bleb or by internal membrane vesicles (Fig. 5f and g). The function and composition of the cone structure in this and other spirochetes are currently unknown. One can speculate that the cone (Fig. 8, purple) may have extensions across the outer membrane and may be involved in adherence or sensory functions; however, studies of the resident protein(s) and/or other components and their properties are needed to elucidate the possible roles of this unique and fascinating structure.

Materials and Methods

Ethics statement

All procedures involving rabbits were reviewed and approved by the Animal Welfare Committee of the University of Texas Health Science Center at Houston.

Cryo-ET of intact *T. pallidum*

T. pallidum subsp. *pallidum* Nichols was extracted from rabbit testes after intratesticular infection; in some experiments, the organisms were further purified by Percoll density gradient centrifugation, as described previously.[20] Freshly prepared motile *T. pallidum* was centrifuged and resuspended in 20 μl of phosphate-buffered saline (PBS) at a final concentration of $\sim 2 \times 10^9$ cells/ml. The 4-μl samples of *T. pallidum*, after mixing with 10-nm gold clusters, were deposited onto freshly glow-discharged holey carbon grids for 1 min. The grids were blotted with filter paper and rapidly frozen in liquid ethane maintained at −180 °C using a gravity-driven plunger apparatus, as previously described.[44] The resulting frozen–hydrated specimens were imaged at −170 °C using a Polara G2 electron microscope (FEI Company) equipped with a field emission gun and a 4000 × 4000 charge-coupled device (16-megapixel) camera (TVIPS GmbH, Germany). The microscope was operated at 300 kV at a magnification of 31,000×, resulting in an effective pixel size of 2.8 Å. Using the FEI "batch tomography" program, we collected low-dose single-axis tilt series from each bacterium at a defocus of −4 μm to −6 μm with a cumulative dose of $\sim 100\ e^-/Å^2$ distributed over 65 images, covering an angular range from −64° to +64° at angular increments of 2°. A 30-μm objective aperture and a 2 × 2 binning of pixels were used to enhance the image contrast at this defocus level. Tilted images were initially aligned with respect to each other using fiducial markers and the IMOD software package.[68] After further refinement using projection matching, 3D tomograms were reconstructed using weighted backprojection implemented in the package Protomo.[69] In total, 304 cryotomograms from *T. pallidum* cells were reconstructed. The effective pixel size of tomographic reconstructions is 5.6 Å, and the effective in-plane resolution is better than 4 nm, based on the direct separation of lipid bilayers. A 2 × 2 × 2 binning of these tomograms was used for the visualization of 3D images and the preparation of figures.

Outer membrane removal, surface proteolysis, and lysozyme treatment

Percoll-purified *T. pallidum* organisms in PBS ($\sim 1 \times 10^9$) were centrifuged at 21,000*g* for 1 min, resuspended in 500 μl of PBS with 5 mM $MgCl_2$, and pipetted vigorously ~20 times. This process was repeated. As a result of this treatment, the outer membrane was removed from the majority of *T. pallidum* organisms. Surface proteolysis was carried out on this preparation by treatment with proteinase K (0.4 mg/ml) for 40 min at ambient temperature, as described by Liu *et al.*[44] The same preparation was treated in parallel with lysozyme (0.6 mg/ml).

Immunogold labeling of flagellar filaments

Percoll-purified *T. pallidum* cells partially disrupted by repeated centrifugation, as described above, were applied to carbon-coated grids and incubated with PBS containing 5% bovine serum albumin (BSA) for 30 min, followed by washing with PBS–5% BSA. Grids were placed on a 30-μl drop of primary rabbit antisera against either FlaA or FlaB1[32] diluted 1:20 in PBS–5% BSA for 60 min, followed by washing with PBS–5% BSA three times. The samples were stained with gold goat anti-rabbit immunoglobulin G (Jackson ImmunoResearch) diluted 1:20 in PBS–5% BSA for 60 min, followed by washing with PBS–2% BSA. The grids were washed with water before staining with 1% uranyl acetate. Samples were viewed with a JEM1200 electron microscope.

Subvolume averaging of flagellar motor and filament

The subvolume processing of flagellar motors was carried out as described by Liu *et al.*[44] The positions and orientations of each flagellar motor in each tomogram were determined manually. Subvolumes (256 × 256 × 256 voxels) containing entire flagellar motors were extracted from the original tomograms. In total, 830 flagellar motor volumes were extracted from 273 tomograms and further used for 3D alignment, classification, and averaging. The resolution of the flagellar motor structure is 4.0 nm based on the Fourier shell correlation (cutoff, 0.5).

A total of 4166 segments (192 × 192 × 96 voxels) of flagellar filaments were manually identified and extracted from 55 reconstructions. The initial orientation was determined using two adjacent points along the filament. The first one is proximal to the flagellar hook, and the polarity of the filament was preserved during the alignment process. After obtaining the asymmetric reconstruction of the flagellar filament, we determined and imposed the helical symmetry of the short segment. The helical model was then used as reference for further 3D alignment and averaging.

Three-dimensional visualization

Tomographic reconstructions were visualized using IMOD,[68] and surface rendering of flagellar structures was carried out with the software package UCSF Chimera.[70] Reconstructions of several *T. pallidum* organisms were segmented manually using the 3D modeling software Amira (Visage Imaging). Three-dimensional segmentation of the flagellar filaments, cytoplasmic filaments, outer and cytoplasmic membranes, and unique cone-shaped structure was manually constructed. The surface model from the averaged flagellar motor was computationally mapped back into the original cellular context, as described previously.[71]

Scanning probe microscopy

SPM was carried out using a Digital Instruments/Veeco MultiMode™ instrument equipped with a Nanoscope IIIa SPM controller. A cantilever probe with a spring constant of 40 N/m and an inherent resonance (f_0) of ~300 kHz was used. Freshly extracted *T. pallidum* ($6 \times 10^6\ ml^{-1}$) in PBS was centrifuged at 500*g* for 5 min to remove host cell debris and fixed in 3% glutaraldehyde. A 10-μl sample was applied to a mica support and air dried. The specimen was rinsed three times with distilled water and air dried prior to SPM. Scanning was performed in tapping mode at a scan rate of one line per second.

Acknowledgements

We thank Drs. James K. Stoops, Angel Paredes, Hanspeter Winkler, Ken Taylor, and Douglas Botkin for their comments and suggestions. We also thank Matthew Swulius for advice and assistance with immunogold labeling. This work was supported, in part, by Welch Foundation grant AU-1714 and National Institutes of Health grant 1R01AI087946 (to J.L.). Maintenance of the Polara electron microscope facility was supported by the Structural Biology Center at the University of Texas Medical School at Houston.

Supplementary Data

Supplementary data to this article can be found online at doi:10.1016/j.jmb.2010.09.020

References

1. Gerbase, A. C., Rowley, J. T., Heymann, D. H., Berkley, S. F. & Piot, P. (1998). Global prevalence and incidence estimates of selected curable STDs. *Sex. Transm. Infect.* **74**, S12–S16.
2. Lafond, R. E. & Lukehart, S. A. (2006). Biological basis for syphilis. *Clin. Microbiol. Rev.* **19**, 29–49.
3. Galvin, S. R. & Cohen, M. S. (2004). The role of sexually transmitted diseases in HIV transmission. *Nat. Rev. Microbiol.* **2**, 33–42.
4. Norris, S. J., Paster, B. J., Moter, A. & Gobel, U. B. (2006). The genus *Treponema*. In *The Prokaryotes: Vol. 7. Proteobacteria: Delta, Epsilon Subclass* (Dworkin, M., Falkow, S., Rosenberg, E., Schleifer, K.-H., Stackebrandt, E. & SpringerLink (Online Service), eds), Springer-Verlag, New York, NY.
5. Fraser, C. M., Norris, S. J., Weinstock, G. M., White, O., Sutton, G. G., Dodson, R. *et al.* (1998). Complete genome sequence of *Treponema pallidum*, the syphilis spirochete. *Science*, **281**, 375–388.
6. Matejkova, P., Strouhal, M., Smajs, D., Norris, S. J., Palzkill, T., Petrosino, J. F. *et al.* (2008). Complete genome sequence of *Treponema pallidum* ssp. *pallidum* strain SS14 determined with oligonucleotide arrays. *BMC Microbiol.* **8**, 76.
7. Norris, S. J. & Edmondson, D. G. (1986). Factors affecting the multiplication and subculture of *Treponema pallidum* subsp. *pallidum* in a tissue culture system. *Infect. Immun.* **53**, 534–539.
8. Steere, A. C., Coburn, J. & Glickstein, L. (2004). The emergence of Lyme disease. *J. Clin. Invest.* **113**, 1093–1101.
9. Levett, P. N. (2001). Leptospirosis. *Clin. Microbiol. Rev.* **14**, 296–326.
10. Charon, N. W. & Goldstein, S. F. (2002). Genetics of motility and chemotaxis of a fascinating group of bacteria: the spirochetes. *Annu. Rev. Genet.* **36**, 47–73.
11. Norris, S. J. (1993). Polypeptides of *Treponema pallidum*: progress toward understanding their structural, functional, and immunologic roles. *Treponema pallidum* Polypeptide Research Group. *Microbiol. Rev.* **57**, 750–779.
12. Fraser, C. M., Casjens, S., Huang, W. M., Sutton, G. G., Clayton, R., Lathigra, R. *et al.* (1997). Genomic sequence of a Lyme disease spirochaete, *Borrelia burgdorferi*. *Nature*, **390**, 580–586.
13. Johnson, R. C., Ritzi, D. M. & Livermore, B. P. (1973). Outer envelope of virulent *Treponema pallidum*. *Infect. Immun.* **8**, 291–295.
14. Hovind-Hougen, K. (1976). Determination by means of electron microscopy of morphological criteria of value for classification of some spirochetes, in particular treponemes. *Acta Pathol. Microbiol. Scand. Suppl.* 1–41.
15. Walker, E. M., Zampighi, G. A., Blanco, D. R., Miller, J. N. & Lovett, M. A. (1989). Demonstration of rare protein in the outer membrane of *Treponema pallidum* subsp. *pallidum* by freeze-fracture analysis. *J. Bacteriol.* **171**, 5005–5011.
16. Radolf, J. D., Norgard, M. V. & Schulz, W. W. (1989). Outer membrane ultrastructure explains the limited antigenicity of virulent *Treponema pallidum*. *Proc. Natl Acad. Sci. USA*, **86**, 2051–2055.
17. Izard, J. (2006). Cytoskeletal cytoplasmic filament ribbon of *Treponema*: a member of an intermediate-like filament protein family. *J. Mol. Microbiol. Biotechnol.* **11**, 159–166.
18. Izard, J., McEwen, B. F., Barnard, R. M., Portuese, T., Samsonoff, W. A. & Limberger, R. J. (2004). Tomographic reconstruction of treponemal cytoplasmic filaments reveals novel bridging and anchoring components. *Mol. Microbiol.* **51**, 609–618.
19. Izard, J., Samsonoff, W. A. & Limberger, R. J. (2001). Cytoplasmic filament-deficient mutant of *Treponema denticola* has pleiotropic defects. *J. Bacteriol.* **183**, 1078–1084.
20. You, Y., Elmore, S., Colton, L. L., Mackenzie, C., Stoops, J. K., Weinstock, G. M. & Norris, S. J. (1996). Characterization of the cytoplasmic filament protein gene (cfpA) of *Treponema pallidum* subsp. *pallidum*. *J. Bacteriol.* **178**, 3177–3187.
21. Setubal, J. C., Reis, M., Matsunaga, J. & Haake, D. A. (2006). Lipoprotein computational prediction in spirochaetal genomes. *Microbiology*, **152**, 113–121.
22. Radolf, J. D. (1994). Role of outer membrane architecture in immune evasion by *Treponema pallidum* and *Borrelia burgdorferi*. *Trends Microbiol.* **2**, 307–311.
23. Radolf, J. D. & Desrosiers, D. C. (2009). *Treponema pallidum*, the stealth pathogen, changes, but how? *Mol. Microbiol.* **72**, 1081–1086.
24. Berg, H. C. (2003). The rotary motor of bacterial flagella. *Annu. Rev. Biochem.* **72**, 19–54.
25. Macnab, R. M. (2003). How bacteria assemble flagella. *Annu. Rev. Microbiol.* **57**, 77–100.
26. Kojima, S. & Blair, D. F. (2004). The bacterial flagellar motor: structure and function of a complex molecular machine. *Int. Rev. Cytol.* **233**, 93–134.
27. Sowa, Y. & Berry, R. M. (2008). Bacterial flagellar motor. *Q. Rev. Biophys.* **41**, 103–132.
28. Terashima, H., Kojima, S. & Homma, M. (2008). Flagellar motility in bacteria structure and function of flagellar motor. *Int. Rev. Cell Mol. Biol.* **270**, 39–85.
29. Goldstein, S. F., Li, C., Liu, J., Miller, M., Motaleb, M. A., Norris, S. J. *et al.* (2010). The chic motility and

chemotaxis of *Borrelia burgdorferi*. In *Borrelia: Molecular Biology, Host Interaction and Pathogenesis* (Samuels, D. S. & Radolf, J. D., eds), Caister Academic Press, Norfolk, UK.
30. Li, C., Bakker, R. G., Motaleb, M. A., Sartakova, M. L., Cabello, F. C. & Charon, N. W. (2002). Asymmetrical flagellar rotation in *Borrelia burgdorferi* nonchemotactic mutants. *Proc. Natl Acad. Sci. USA*, **99**, 6169–6174.
31. Cockayne, A., Bailey, M. J. & Penn, C. W. (1987). Analysis of sheath and core structures of the axial filament of *Treponema pallidum*. *J. Gen. Microbiol.* **133**, 1397–1407.
32. Norris, S. J., Charon, N. W., Cook, R. G., Fuentes, M. D. & Limberger, R. J. (1988). Antigenic relatedness and N-terminal sequence homology define two classes of periplasmic flagellar proteins of *Treponema pallidum* subsp. *pallidum* and *Treponema phagedenis*. *J. Bacteriol.* **170**, 4072–4082.
33. Radolf, J. D., Blanco, D. R., Miller, J. N. & Lovett, M. A. (1986). Antigenic interrelationship between endoflagella of *Treponema phagedenis* biotype Reiter and *Treponema pallidum* (Nichols): molecular characterization of endoflagellar proteins. *Infect. Immun.* **54**, 626–634.
34. Izard, J., Hsieh, C. E., Limberger, R. J., Mannella, C. A. & Marko, M. (2008). Native cellular architecture of *Treponema denticola* revealed by cryo-electron tomography. *J. Struct. Biol.* **163**, 10–17.
35. Izard, J., Renken, C., Hsieh, C. E., Desrosiers, D. C., Dunham-Ems, S., La Vake, C. *et al.* (2009). Cryo-electron tomography elucidates the molecular architecture of *Treponema pallidum*, the syphilis spirochete. *J. Bacteriol.* **191**, 7566–7580.
36. Kudryashev, M., Cyrklaff, M., Baumeister, W., Simon, M. M., Wallich, R. & Frischknecht, F. (2009). Comparative cryo-electron tomography of pathogenic Lyme disease spirochetes. *Mol. Microbiol.* **71**, 1415–1434.
37. Murphy, G. E., Matson, E. G., Leadbetter, J. R., Berg, H. C. & Jensen, G. J. (2008). Novel ultrastructures of *Treponema primitia* and their implications for motility. *Mol. Microbiol.* **67**, 1184–1195.
38. Baumeister, W. (2005). From proteomic inventory to architecture. *FEBS Lett.* **579**, 933–937.
39. Nickell, S., Kofler, C., Leis, A. P. & Baumeister, W. (2006). A visual approach to proteomics. *Nat. Rev. Mol. Cell Biol.* **7**, 225–230.
40. Liu, J., Bartesaghi, A., Borgnia, M. J., Sapiro, G. & Subramaniam, S. (2008). Molecular architecture of native HIV-1 gp120 trimers. *Nature*, **455**, 109–113.
41. Liu, J., Taylor, D. W., Krementsova, E. B., Trybus, K. M. & Taylor, K. A. (2006). Three-dimensional structure of the myosin V inhibited state by cryoelectron tomography. *Nature*, **442**, 208–211.
42. Liu, J., Wu, S., Reedy, M. C., Winkler, H., Lucaveche, C., Cheng, Y. *et al.* (2006). Electron tomography of swollen rigor fibers of insect flight muscle reveals a short and variably angled S2 domain. *J. Mol. Biol.* **362**, 844–860.
43. Winkler, H. (2007). 3D reconstruction and processing of volumetric data in cryo-electron tomography. *J. Struct. Biol.* **157**, 126–137.
44. Liu, J., Lin, T., Botkin, D. J., McCrum, E., Winkler, H. & Norris, S. J. (2009). Intact flagellar motor of *Borrelia burgdorferi* revealed by cryo-electron tomography: evidence for stator ring curvature and rotor/C-ring assembly flexion. *J. Bacteriol.* **191**, 5026–5036.
45. Briegel, A., Ortega, D. R., Tocheva, E. I., Wuichet, K., Li, Z., Chen, S. *et al.* (2009). Universal architecture of bacterial chemoreceptor arrays. *Proc. Natl Acad. Sci. USA*, **106**, 17181–17186.
46. Radmacher, M., Tillamnn, R. W., Fritz, M. & Gaub, H. E. (1992). From molecules to cells: imaging soft samples with the atomic force microscope. *Science*, **257**, 1900–1905.
47. Walker, E. M., Borenstein, L. A., Blanco, D. R., Miller, J. N. & Lovett, M. A. (1991). Analysis of outer membrane ultrastructure of pathogenic *Treponema* and *Borrelia* species by freeze-fracture electron microscopy. *J. Bacteriol.* **173**, 5585–5588.
48. Murphy, G. E., Leadbetter, J. R. & Jensen, G. J. (2006). *In situ* structure of the complete *Treponema primitia* flagellar motor. *Nature*, **442**, 1062–1064.
49. Li, C., Corum, L., Morgan, D., Rosey, E. L., Stanton, T. B. & Charon, N. W. (2000). The spirochete FlaA periplasmic flagellar sheath protein impacts flagellar helicity. *J. Bacteriol.* **182**, 6698–6706.
50. Hazlett, K. R., Cox, D. L., Decaffmeyer, M., Bennett, M. P., Desrosiers, D. C., La Vake, C. J. *et al.* (2005). TP0453, a concealed outer membrane protein of *Treponema pallidum*, enhances membrane permeability. *J. Bacteriol.* **187**, 6499–6508.
51. Charon, N. W., Goldstein, S. F., Marko, M., Hsieh, C., Gebhardt, L. L., Motaleb, M. A. *et al.* (2009). The flat-ribbon configuration of the periplasmic flagella of *Borrelia burgdorferi* and its relationship to motility and morphology. *J. Bacteriol.* **191**, 600–607.
52. Cox, D. L., Chang, P., McDowall, A. W. & Radolf, J. D. (1992). The outer membrane, not a coat of host proteins, limits antigenicity of virulent *Treponema pallidum*. *Infect. Immun.* **60**, 1076–1083.
53. Radolf, J. D., Bourell, K. W., Akins, D. R., Brusca, J. S. & Norgard, M. V. (1994). Analysis of *Borrelia burgdorferi* membrane architecture by freeze-fracture electron microscopy. *J. Bacteriol.* **176**, 21–31.
54. Cameron, C. E. (2006). *T. pallidum* outer membrane and outer membrane proteins. In *Pathogenic Treponema: Molecular and Cellular Biology* (Radolf, J. D. & Lukehart, S. A., eds), Caister Academic, Wymondham, Norfolk, UK.
55. Brandt, M. E., Riley, B. S., Radolf, J. D. & Norgard, M. V. (1990). Immunogenic integral membrane proteins of *Borrelia burgdorferi* are lipoproteins. *Infect. Immun.* **58**, 983–991.
56. Porcella, S. F. & Schwan, T. G. (2001). *Borrelia burgdorferi* and *Treponema pallidum*: a comparison of functional genomics, environmental adaptations, and pathogenic mechanisms. *J. Clin. Invest.* **107**, 651–656.
57. Chamberlain, N. R., Brandt, M. E., Erwin, A. L., Radolf, J. D. & Norgard, M. V. (1989). Major integral membrane protein immunogens of *Treponema pallidum* are proteolipids. *Infect. Immun.* **57**, 2872–2877.
58. Brinkman, M. B., McGill, M. A., Pettersson, J., Rogers, A., Matejkova, P., Smajs, D. *et al.* (2008). A novel *Treponema pallidum* antigen, TP0136, is an outer membrane protein that binds human fibronectin. *Infect. Immun.* **76**, 1848–1857.

59. Centurion-Lara, A., Castro, C., Barrett, L., Cameron, C., Mostowfi, M., Van Voorhis, W. C. & Lukehart, S. A. (1999). *Treponema pallidum* major sheath protein homologue Tpr K is a target of opsonic antibody and the protective immune response. *J. Exp. Med.* **189**, 647–656.
60. Cullen, P. A. & Cameron, C. E. (2006). Progress towards an effective syphilis vaccine: the past, present and future. *Expert Rev. Vaccines*, **5**, 67–80.
61. Yonekura, K., Maki-Yonekura, S. & Namba, K. (2003). Complete atomic model of the bacterial flagellar filament by electron cryomicroscopy. *Nature*, **424**, 643–650.
62. Galkin, V. E., Yu, X., Bielnicki, J., Heuser, J., Ewing, C. P., Guerry, P. & Egelman, E. H. (2008). Divergence of quaternary structures among bacterial flagellar filaments. *Science*, **320**, 382–385.
63. Li, C., Wolgemuth, C. W., Marko, M., Morgan, D. G. & Charon, N. W. (2008). Genetic analysis of spirochete flagellin proteins and their involvement in motility, filament assembly, and flagellar morphology. *J. Bacteriol.* **190**, 5607–5615.
64. Pallen, M. J., Penn, C. W. & Chaudhuri, R. R. (2005). Bacterial flagellar diversity in the post-genomic era. *Trends Microbiol.* **13**, 143–149.
65. Yang, Y., Stewart, P. E., Shi, X. & Li, C. (2008). Development of a transposon mutagenesis system in the oral spirochete *Treponema denticola*. *Appl. Environ. Microbiol.* **74**, 6461–6464.
66. Izard, J., Samsonoff, W. A., Kinoshita, M. B. & Limberger, R. J. (1999). Genetic and structural analyses of cytoplasmic filaments of wild-type *Treponema phagedenis* and a flagellar filament-deficient mutant. *J. Bacteriol.* **181**, 6739–6746.
67. Masuda, K. & Kawata, T. (1989). Isolation and characterization of cytoplasmic fibrils from treponemes. *Microbiol. Immunol.* **33**, 619–630.
68. Kremer, J. R., Mastronarde, D. N. & McIntosh, J. R. (1996). Computer visualization of three-dimensional image data using IMOD. *J. Struct. Biol.* **116**, 71–76.
69. Winkler, H. & Taylor, K. A. (2006). Accurate marker-free alignment with simultaneous geometry determination and reconstruction of tilt series in electron tomography. *Ultramicroscopy*, **106**, 240–254.
70. Pettersen, E. F., Goddard, T. D., Huang, C. C., Couch, G. S., Greenblatt, D. M., Meng, E. C. & Ferrin, T. E. (2004). UCSF Chimera—a visualization system for exploratory research and analysis. *J. Comput. Chem.* **25**, 1605–1612.
71. Wu, S., Liu, J., Reedy, M. C., Winkler, H., Reedy, M. K. & Taylor, K. A. (2009). Methods for identifying and averaging variable molecular conformations in tomograms of actively contracting insect flight muscle. *J. Struct. Biol.* **168**, 485–502.